2010 IEEE International Conference on Robotics and Automation
Anchorage Convention District
May 3-8, 2010, Anchorage, Alaska, USA

Simultaneous Calibration of Odometry and Camera for a Differential Drive Mobile Robot

Gianluca Antonelli, Fabrizio Caccavale, Flavio Grossi, Alessandro Marino

Abstract— **Differential-drive mobile robots are usually equipped with video-cameras for navigation purposes. In order to ensure proper operational capabilities of such systems, several calibration steps are required to estimate the following quantities: the video-camera intrinsic and extrinsic parameters, the relative pose between the camera and the vehicle frame and, finally, the odometric parameters of the vehicle. In this paper the simultaneous estimation of the above mentioned quantities is achieved by a systematic and effective calibration procedure that does not require any iterative step.**
The calibration procedure needs only on-board measurements given by the wheels encoders, the camera and a number of properly taken camera snapshots of a set of known landmarks. Numerical simulations and experimental results with a mobile robot Khepera III equipped with a low-cost camera confirm the effectiveness of the proposed technique.

I. Introduction

In the case of differential-drive mobile robots equipped with a video-camera, several calibrations problems need to be tackled: namely, the odometry calibration, the video-camera calibration and the relative vehicle-camera pose calibration.

Odometry is the reconstruction of the mobile robot configuration, i.e., position and orientation, resorting to the encoders' measurements at the wheels. Starting from a known configuration, the current position and orientation of the robot is obtained by time integration of the vehicle's velocity corresponding to wheels' velocity. Video-camera calibration concerns both the intrinsic parameters (e.g., the focal length) and the extrinsic parameters (e.g., the relative pose with respect to an inertial frame). It is a mature topic on which a wide and assessed literature exists [8]. Moreover, when a camera is mounted on a robot, an additional calibration procedure is required; namely, the so-called hand-eye calibration [11], which is aimed at determining the relative pose between the camera and a robot-fixed frame. Although its name is inherited from the specific problem of a camera mounted on the end-effector of a robot manipulator, this step is, of course, required for a camera mounted on a mobile robot as well.

Several research efforts have been focused on the above mentioned calibration problems, although they have been tackled individually; e.g., for odometric calibration, external video-cameras (already calibrated) have been used, while hand-eye calibration is usually solved by resorting to already calibrated robots. Concerning the odometric calibration, starting from [17], there has been an intense research activity; one of the most used algorithms is presented in [3]. Recently, in [6], an algorithm, based on the boundedness property of the error for Generalized-Voronoi-Graph-based paths, has been proposed and experimentally validated. In [7] it is proposed to drive the robot through a known path and then evaluate the shape of the resulting path to estimate the model parameters. The works [13], [14] present a method to identify two systematic and two non-systematic errors. In [9], [10], the error propagation in vehicle odometry is analytically discussed and two main results are given: quadratic dependency of the estimation error with respect to the distance traveled and existence of path-independent systematic errors. In [2] a calibration method aimed at identifying a 4-parameter odometric model has been proposed that shows a linear relation between the unknowns and the measurements; it is thus possible the use of linear estimation tools. In [1] the linear estimation approach developed in [2] is further improved so as to estimate the physical odometric parameters, thus yielding a 3-parameter model. It is worth noticing that all the methods above require external measurement systems such as, e.g., calibrated video-cameras or ranging sensors. Recently, in [4] simultaneous calibration of odometry and range sensors is achieved without resorting to external sensors.

In this paper simultaneous calibration of the intrinsic and extrinsic video-camera parameters, hand-eye and odometric parameters is achieved by a novel, systematic and non-iterative calibration procedure. This procedure only needs on-board measurements given by the wheels encoders, the camera and a number of properly taken camera snapshots of a set of landmarks whose position is known in the inertial frame.

Moreover, differently from other approaches, no specific path is required to be followed: the vehicle is asked to roughly move around the landmarks and acquire a minimum of three snapshots at some approximatively given configurations. In addition, since the whole calibration procedure does not use external measurement devices, it can be used to calibrate, on-site, a team of mobile robots with respect to the same inertial frame, given by the position of the camera calibration tool.

Finally, numerical simulations and experimental results with a mobile robot Khepera III equipped with a low-cost camera confirm the effectiveness of the proposed technique.

G. Antonelli and F. Grossi are with the Dipartimento di Automazione, Elettromagnetismo, Ingegneria dell'Informazione e Matematica Industriale, Università degli Studi di Cassino, Via G. Di Biasio 43, 03043, Cassino (FR), Italy, antonelli@unicas.it.

A. Marino and F. Caccavale are with the Dipartimento di Ingegneria e Fisica dell'Ambiente, Università degli Studi della Basilicata, Viale dell'Ateneo Lucano 10, 85100, Potenza, Italy, {alessandro.marino,fabrizio.caccavale}@unibas.it

II. Background

A. Variables definition

All relevant quantities are listed in the following table (see also Figure 1).

$\Sigma_i - \{\boldsymbol{o}_i, \boldsymbol{x}_i, \boldsymbol{y}_i, \boldsymbol{z}_i\}$	Inertial frame
$\Sigma_v - \{\boldsymbol{o}_v, \boldsymbol{x}_v, \boldsymbol{y}_v, \boldsymbol{z}_v\}$	Vehicle-fixed frame
$\Sigma_c - \{\boldsymbol{o}_c, \boldsymbol{x}_c, \boldsymbol{y}_c, \boldsymbol{z}_c\}$	Camera-fixed frame
x, y, θ	vehicle configuration
v, ω	vehicle linear/angular velocities
ω_R, ω_L	right/left wheel angular velocities
θ_R, θ_L	right/left wheel angular position
r_R, r_L, b	right/left wheel radii, wheelbase
α_R, α_L	intermediate odometric variables
$\boldsymbol{R}_x(\alpha)$	rotation of α around the $\boldsymbol{x}$ axis
$\boldsymbol{R}_l^j \in \mathbb{R}^{3\times3}$	rotation from frame l to frame j
$\boldsymbol{t}_{lj}^l \in \mathbb{R}^3$	vector of the origin of frame j with respect of the origin of frame l expressed in frame l
$\boldsymbol{A}_l^j \in \mathbb{R}^{4\times4}$	homogeneous transformation from frame l to frame j
$\overline{\boldsymbol{x}}$	homogeneous vector of $\boldsymbol{x}$
$\boldsymbol{p}^i \in \mathbb{R}^3$	landmark expr. in inertial frame
$\boldsymbol{p}^c \in \mathbb{R}^3$	landmark expr. in camera frame
$[p_u \quad p_v]^T$	pixel in the image plane
$\boldsymbol{f}_c \in \mathbb{R}^2$	camera focal length expr. in pixel
k_r	radial distortion coefficient
P	number of different poses
$N = P(P-1)/2$	possible combinations of poses

B. Unicycle kinematics

Let x and y the coordinates of the origin of Σ_v, expressed in the frame Σ_i, and θ the heading angle between the x-axes of Σ_v and Σ_i; then, the robot kinematics is given by

$$\begin{cases} \dot{x} = v\cos(\theta) \\ \dot{y} = v\sin(\theta) \\ \dot{\theta} = \omega\,. \end{cases} \tag{1}$$

It can be recognized that (see Figure 1) the body-fixed components, v and ω, of the robot velocity are related to the left and right angular velocity of the wheels, ω_L and ω_R, respectively, by

$$\begin{cases} v = \dfrac{r_R}{2}\,\omega_R + \dfrac{r_L}{2}\,\omega_L \\ \omega = \dfrac{r_R}{b}\,\omega_R - \dfrac{r_L}{b}\,\omega_L, \end{cases} \tag{2}$$

in which r_R and r_L are the radii of the right and left wheels, respectively, and b is the length of the wheels axis.

C. Frames relationships in different vehicle's poses

It is assumed that the vehicle is equipped with an on-board camera, with a corresponding frame Σ_c.

Let us further define as $\boldsymbol{R}_i^c \in \mathbb{R}^{3\times3}$ the rotation matrix from the inertial frame to the camera frame, and as $\boldsymbol{t}_{ci}^c \in \mathbb{R}^3$ the vector of the origin of the inertial frame with respect to the origin of the camera frame, expressed in the camera

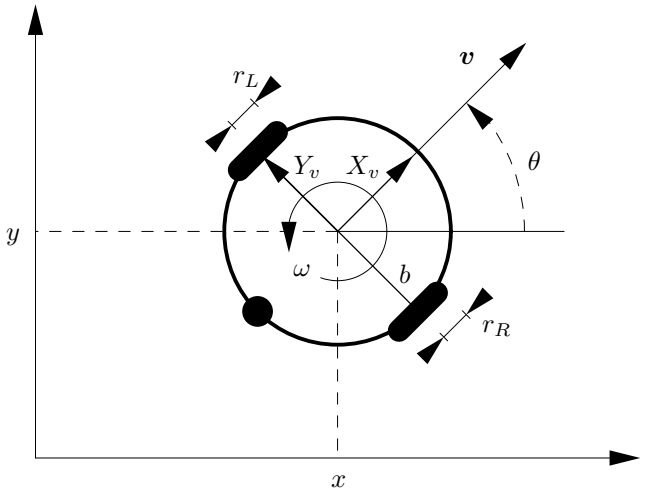

Fig. 1. Top-view sketch of a differential-drive mobile robot with relevant variables.

frame. It is possible to define the following homogeneous transformation matrix

$$\boldsymbol{A}_i^c = \begin{bmatrix} \boldsymbol{R}_i^c & \boldsymbol{t}_{ci}^c \\ \boldsymbol{0}^{\mathrm{T}} & 1 \end{bmatrix} \tag{3}$$

where $\boldsymbol{0}$ is the (3×1) null vector and the homogeneous vector is given by

$$\overline{\boldsymbol{p}}^c = \begin{bmatrix} \boldsymbol{p}^{cT} & 1 \end{bmatrix}^{\mathrm{T}}. \tag{4}$$

The following holds

$$\overline{\boldsymbol{p}}^c = \boldsymbol{A}_i^c \overline{\boldsymbol{p}}^i. \tag{5}$$

Matrices $\boldsymbol{A}_i^v$ and $\boldsymbol{A}_c^v$ can be defined in the same way.
Let us now consider different vehicle *poses*, where the term pose denotes a configuration at which the vehicle is still; a numbered subscript univocally indicates a specific pose. Let us now also introduce the homogeneous transformations $\boldsymbol{A}_{c1}^{c2}$ and $\boldsymbol{A}_{v1}^{v2}$ (see Figure 2), where the subscripts 1 and 2 denote two different poses.

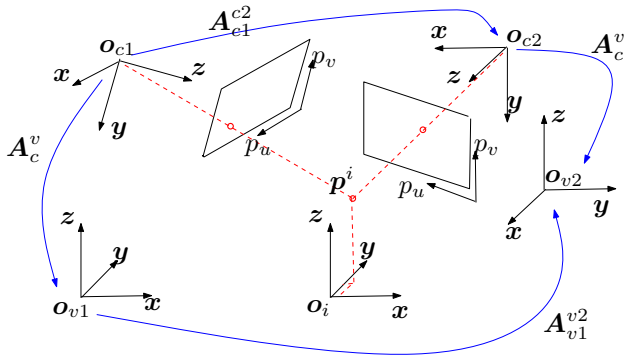

Fig. 2. Sketch with the frames definition

It can be shown that [11], [15]:

$$\boldsymbol{A}_c^v \boldsymbol{A}_{c1}^{c2} = \boldsymbol{A}_{v1}^{v2} \boldsymbol{A}_c^v, \tag{6}$$

where the subscripts 1 and 2, denoting the poses, have been omitted in $\boldsymbol{A}_c^v$, since it is constant. Equation (6) can be decomposed into the rotational and translational parts as follows

$$\begin{aligned} \boldsymbol{R}_c^v \boldsymbol{R}_{c1}^{c2} &= \boldsymbol{R}_{v1}^{v2} \boldsymbol{R}_c^v & (7) \\ \boldsymbol{R}_c^v \boldsymbol{t}_{c2c1}^{c2} - \boldsymbol{t}_{v2v1}^{v2} &= \boldsymbol{R}_{v1}^{v2} \boldsymbol{t}_{vc}^v - \boldsymbol{t}_{vc}^v. & (8) \end{aligned}$$

Assuming that $\boldsymbol{A}_i^c$ is known (it can be obtained, e.g., via a vision calibration procedure) for all the poses, it is possible to write

$$\boldsymbol{A}_{c1}^{c2} = \boldsymbol{A}_i^{c2} \boldsymbol{A}_{c1}^i. \quad (9)$$

As noticed in, e.g., [5], the motion of the vehicle, which is constrained to be planar, does not allow to identify all the unknowns of eq. (6) (or, equivalently, in eqs. (7),(8)). However, the following derivation, inspired by the work in [5], shows how to project (7) to determine the relevant quantities on the basis of the available motion variables. In detail, the vehicle rotates only around the $\boldsymbol{z}_i$-axis of the inertial frame, i.e.,

$$\boldsymbol{R}_{v1}^{v2} = \boldsymbol{R}_z(\theta), \quad (10)$$

where $\boldsymbol{R}_z(\theta)$ is an elementary rotation around the $\boldsymbol{z}$ axis. Hence, eq. (7) becomes:

$$\boldsymbol{R}_v^c \boldsymbol{R}_z(\theta) \boldsymbol{R}_c^v = \boldsymbol{R}_{c1}^{c2}. \quad (11)$$

It is possible to represent the rotation matrix $\boldsymbol{R}_c^v$ in terms of elementary rotations (Euler angles) ZYZ, i.e., $\boldsymbol{R}_c^v = \boldsymbol{R}_z(\alpha_1)\boldsymbol{R}_y(\alpha_2)\boldsymbol{R}_z(\alpha_3)$. Hence, the following holds

$$\boldsymbol{R}_z(-\alpha_3)\boldsymbol{R}_y(-\alpha_2)\boldsymbol{R}_z(-\alpha_1)\boldsymbol{R}_z(\theta)\boldsymbol{R}_z(\alpha_1)\boldsymbol{R}_y(\alpha_2)\boldsymbol{R}_z(\alpha_3) = \boldsymbol{R}_{c1}^{c2}. \quad (12)$$

It is straightforward to demonstrate that the above equation can be simplified as

$$\boldsymbol{R}_z(-\alpha_3)\boldsymbol{R}_y(-\alpha_2)\boldsymbol{R}_z(\theta)\boldsymbol{R}_y(\alpha_2)\boldsymbol{R}_z(\alpha_3) = \boldsymbol{R}_{c1}^{c2}. \quad (13)$$

The left-hand side of (13) corresponds to the definition of axis-angle representation of the orientation [16] (with the proper angles' sign). Assuming $\boldsymbol{R}_{c1}^{c2}$ known, all the characteristic quantities of the left-hand side of (13), i.e., θ, α_2 and α_3, can be computed. In detail [16]:

$$\theta = \cos^{-1}\left(\frac{r_{11} + r_{22} + r_{33} - 1}{2}\right), \quad (14)$$

where r_{ij} denotes the generic element of $\boldsymbol{R}_{c1}^{c2}$. The rotation axis

$$\boldsymbol{r} = \begin{bmatrix} r_x \\ r_y \\ r_z \end{bmatrix} = \frac{1}{2\sin\theta}\begin{bmatrix} r_{32} - r_{23} \\ r_{13} - r_{31} \\ r_{21} - r_{12} \end{bmatrix} \quad (15)$$

allows to compute α_2 and α_3:

$$\begin{aligned} \alpha_2 &= \text{atan2}(\sqrt{r_x^2 + r_y^2}, r_z) & (16) \\ \alpha_3 &= \text{atan2}(r_y, -r_x). & (17) \end{aligned}$$

From eq. (13) it can be noticed that $\theta \neq 0$ is required to avoid a trivial equation satisfied for every axis-angle couple. The physical interpretation is obvious: a nontrivial vehicle rotation is needed to estimate the relevant variables of the left hand side of (13).

D. Pinhole model

The camera model corresponds to a standard pin-hole projection with radial distortion truncated at the first term as reported in [8]. Let

$$\boldsymbol{f}_c = \begin{bmatrix} f_{c,u} & f_{c,v} \end{bmatrix}^{\mathrm{T}} \in \mathbb{R}^2$$

be the effective focal lengths,

$$\boldsymbol{c}_c = \begin{bmatrix} c_{c,u} & c_{c,v} \end{bmatrix}^{\mathrm{T}} \in \mathbb{R}^2$$

be the principal point, both expressed in pixels, and k_r be the radial distortion coefficient. The vector

$$\boldsymbol{p}^c = \begin{bmatrix} x^c & y^c & z^c \end{bmatrix}^{\mathrm{T}} \in \mathbb{R}^3$$

is a point in the camera reference frame, expressed in meter. The pin-hole projection is defined by the following equations

$$\begin{aligned} p_u &= f_{c,u}\left\{1 + k_r\left[\left(\frac{x^c}{z^c}\right)^2 + \left(\frac{y^c}{z^c}\right)^2\right]\right\}\frac{x^c}{z^c} + c_{c,u} \\ p_v &= f_{c,v}\left[1 + k_r\left[\left(\frac{x^c}{z^c}\right)^2 + \left(\frac{y^c}{z^c}\right)^2\right]\right]\frac{y^c}{z^c} + c_{c,v}\,, \end{aligned}$$

where p_u and p_v are the pixels coordinates. Of course, the given point can be expressed in a different reference frame, e.g., the inertial frame, by the known relation (in homogeneous coordinates)

$$\overline{\boldsymbol{p}}^i = \boldsymbol{A}_c^i \overline{\boldsymbol{p}}^c.$$

III. Problem formulation and proposed solution

Let us assume that the following sensing devices are available

- incremental or absolute encoders mounted at the shafts of both vehicle wheels;
- a video-camera mounted on the vehicle body.

Additional (external) sensing devices are not necessary. Moreover, it is assumed that a set of landmarks, of known inertial positions, are provided.

It is required to calibrate, simultaneously, the vehicle's odometry (3 parameters: r_R, r_L and b), the intrinsic camera parameters (3 parameters: $\boldsymbol{f}_c$ and k_r) and the camera-vehicle homogeneous transformation (the 6 independent parameters in $\boldsymbol{A}_c^v$). Also, the extrinsic camera parameters (the 6 independent parameters in $\boldsymbol{A}_i^{cj}$ for pose j) are needed.
The solution consists in moving the robot in P configurations (poses); in each pose an image of the landmarks is acquired, during the motion the encoders data are recorded.

The following steps, detailed in next subsections, are then implemented: camera calibration for each pose, estimation of two suitably defined intermediate odometric parameters, estimation of angles α_2, α_3 in $\boldsymbol{R}_c^v$, estimation of the remaining parameters.

A. Step 1: Camera calibration

For each of the P poses an independent camera calibration procedure is set-up. The intrinsic parameters $\boldsymbol{f}_c$ and k_r, as well as the homogeneous transformation matrices $\boldsymbol{A}_i^{cj}$ for $j = \{1, \ldots, P\}$, are then estimated. Vision calibration is an assessed topic in the literature and the several effective algorithm can be adopted; in this paper the calibration is performed with an algorithm based on the minimization of a proper objective function by resorting to the Gauss-Newton method, see, e.g., [12].
It is worth noticing that, once matrices $\boldsymbol{A}_i^{cj}$ are estimated, all the matrices $\boldsymbol{A}_{cj}^{ck}$ (with $j, k = \{1, \ldots, P\}$), expressing the relative configuration between poses j and k can be computed.

B. Step 2: Estimation of intermediate odometric parameters

In order to obtain a linear-in-the-parameters relationship describing the vehicle odometry, the following parameters are defined [1]

$$\alpha_R = \frac{r_R}{b}\,, \quad \alpha_L = -\frac{r_L}{b}, \tag{18}$$

which implies $r_R = -\frac{\alpha_R}{\alpha_L} r_L$. Eq. (18) allows to rewrite the angular velocity as follows

$$\omega = \alpha_R \omega_R + \alpha_L \omega_L\,. \tag{19}$$

By integrating (19) between time instants $t_1 = 0$ and $t_2 = t$, and assuming, without loss of generality, $\theta(0) = 0$, one obtains

$$\theta(t) = \alpha_R \int_0^t \omega_R(\tau)\mathrm{d}\tau + \alpha_L \int_0^t \omega_L(\tau)\mathrm{d}\tau, \tag{20}$$

which can be rewritten as

$$\theta(t) = \alpha_R \theta_R(t) + \alpha_L \theta_L(t)\,, \tag{21}$$

where $\theta_R(t)$, $\theta_L(t)$ represent the encoder positions of the right and left wheel, respectively. The linear relationship between the coefficients α_R, α_L and θ is obvious; in fact, at the generic time instant $t = t_i$ it is possible to write

$$\theta_i = \boldsymbol{\Phi}_{\theta_i} \begin{bmatrix} \alpha_R \\ \alpha_L \end{bmatrix}, \tag{22}$$

with $\theta_i = \theta(t_i)$ and $\boldsymbol{\Phi}_{\theta_i} = \begin{bmatrix} \theta_R(t_i) & \theta_L(t_i) \end{bmatrix}$.
Given N different couple of poses (j, k), the angles θ_i can be measured from the relative camera orientation matrix (i.e., $\boldsymbol{R}_{cj}^{ck}$) by using eq. (14) in Section II-C and considering that the camera and vehicle frames perform the same orientations around tha vertical inertial axis $\boldsymbol{z}_i$. By collecting $N \geq 2$ samples θ_i, equation (22) gives

$$\begin{bmatrix} \theta_1 \\ \vdots \\ \theta_N \end{bmatrix} = \begin{bmatrix} \boldsymbol{\Phi}_{\theta_1} \\ \vdots \\ \boldsymbol{\Phi}_{\theta_N} \end{bmatrix} \begin{bmatrix} \alpha_R \\ \alpha_L \end{bmatrix} = \overline{\boldsymbol{\Phi}}_\theta \begin{bmatrix} \alpha_R \\ \alpha_L \end{bmatrix}. \tag{23}$$

The reconstruction error over the angle data collected in the N samples is then minimized in a least-squares sense by estimating the unknown parameters α_R and α_L as

$$\begin{bmatrix} \hat{\alpha}_R \\ \hat{\alpha}_L \end{bmatrix} = \left(\overline{\boldsymbol{\Phi}}_\theta^{\mathrm{T}} \overline{\boldsymbol{\Phi}}_\theta \right)^{-1} \overline{\boldsymbol{\Phi}}_\theta^{\mathrm{T}} \begin{bmatrix} \theta_1 \\ \vdots \\ \theta_N \end{bmatrix}. \tag{24}$$

It must be noticed that $P \geq 3$ poses are required to perform this step, so as to obtain $N \geq 2$ samples of θ. In addition, it can be easily verified that, if the measured rotations angles are equal or multiple of each other, the regressor is numerically badly scaled. From a practical point of view, this is simply avoided by selecting asymmetric poses around the landmarks.

C. Step 3: Estimation of α_2 and α_3

Angles α_2 and α_3 in (13) can be computed from matrix $\boldsymbol{R}_{cj}^{ck}$, taken in different couple of poses (j, k), by using eqs. (15)–(17) in Section II-C.

It must be noticed that at least $P = 2$ poses are required to estimate $\boldsymbol{r}$, α_2 and α_3. Of course, a larger number of poses may be exploited by properly combining the various estimations.

D. Step 4: Estimation of α_1, $\boldsymbol{t}_{vc}^v$ and r_L

In order to estimate the last angle α_1 in $\boldsymbol{R}_c^v$, $\boldsymbol{t}_{vc}^v$ (only the planar components) and r_L, eq. (8) has to be used. The unidentifiability of the vertical component of $\boldsymbol{t}_{vc}^v$ (i.e., along the z-axis of the inertial frame) can be understood by direct observation of eq. (8), since the third equation is identically satisfied (see [5]).

Let us now rewrite some of terms to better appreciate the dependency from the unknown variables. Vector $\boldsymbol{t}_{c2c1}^{c2}$ is known from the step 1, i.e., the vision calibration, by resorting to the relationship (9). The rotation matrix $\boldsymbol{R}_c^v$, expressed in terms of three elementary rotations $\boldsymbol{R}_c^v = \boldsymbol{R}_z(\alpha_1)\boldsymbol{R}_y(\alpha_2)\boldsymbol{R}_z(\alpha_3)$, is a function of the unknown α_1, since α_2 and α_3 are already available from step 3. Vector $\boldsymbol{t}_{v2v1}^{v2}$ represents the vehicle displacement between two generic poses, expressed with respect to the final frame. Integration of eq. (1) gives the displacement expressed in the initial pose, $\boldsymbol{t}_{v2v1}^{v1}$. Namely, as shown in [1], the following discrete-time equations for the position displacement can be devised from (1)

$$\begin{bmatrix} x_{k+1} - x_k \\ y_{k+1} - y_k \end{bmatrix} = \frac{T}{2} \begin{bmatrix} \left(-\frac{\alpha_R}{\alpha_L} \omega_{R,k} + \omega_{L,k} \right) \cos\left(\theta_k + T\omega_k/2 \right) \\ \left(-\frac{\alpha_R}{\alpha_L} \omega_{R,k} + \omega_{L,k} \right) \sin\left(\theta_k + T\omega_k/2 \right) \end{bmatrix} r_L,$$

where the subscript k denotes the k-th time sample and T is the sampling period. Clearly, the above equation defines a linear mapping between r_L and the position displacement. In particular, the relationship between the kinematic quantities at the initial time step (corresponding to pose 1), $k = 0$, and

final time step (corresponding to pose 2), $k = K$, is

$$\begin{bmatrix} x_K - x_0 \\ y_K - y_0 \end{bmatrix} = \frac{T}{2} \begin{bmatrix} -\frac{\alpha_R}{\alpha_L} \sum_{i=0}^{K-1} \omega_{R,i} c_i + \sum_{i=0}^{K-1} \omega_{L,i} c_i \\ -\frac{\alpha_R}{\alpha_L} \sum_{i=0}^{K-1} \omega_{R,i} s_i + \sum_{i=0}^{K-1} \omega_{L,i} s_i \end{bmatrix} r_L, \quad (25)$$

where $c_i = \cos\Big(\theta_i + T\omega_i/2\Big)$ and $s_i = \sin\Big(\theta_i + T\omega_i/2\Big)$. It is worth noticing that vehicle's orientation angles θ_i can be computed, being α_R and α_L already identified.

Eq. (25) can be rewritten compactly as

$$\boldsymbol{t}_{v1v2}^{v1} = \begin{bmatrix} \beta_1 \\ \beta_2 \\ 0 \end{bmatrix} r_L, \quad (26)$$

with an implicit definition of the two coefficients β_1 and β_2. Eq. (8) can now be rewritten as follows

$$\boldsymbol{R}_c^v \boldsymbol{t}_{c2c1}^{c2} + \boldsymbol{R}_{v1}^{v2} \begin{bmatrix} \beta_1 \\ \beta_2 \\ 0 \end{bmatrix} r_L - \left(\boldsymbol{R}_{v1}^{v2} - \boldsymbol{I}\right) \boldsymbol{t}_{vc}^{v} = \boldsymbol{0}. \quad (27)$$

The first two components of the above equation are those to be considered for the estimation of the unknown parameters. Indeed, the left-hand side of the above equation contains $\boldsymbol{R}_c^v$, that is nonlinear with respect to α_1. However, the term $\boldsymbol{R}_c^v \boldsymbol{t}_{c2c1}^{c2}$ can be rewritten in a form linear in $\sin(\alpha_1)$ and $\cos(\alpha_1)$. Hence, the first two components of eq. (27) can be rewritten in a form linear in the unknown parameters

$$\begin{bmatrix} c_\theta\beta_1 - s_\theta\beta_2 & 1 - c_\theta & s_\theta & a & -b \\ s_\theta\beta_1 + c_\theta\beta_2 & -s_\theta & 1 - c_\theta & b & a \end{bmatrix} \begin{bmatrix} r_L \\ t_{vc,x}^v \\ t_{vc,y}^v \\ c_{\alpha_1} \\ s_{\alpha_1} \end{bmatrix} = \boldsymbol{0}, \quad (28)$$

with $a = c_{\alpha_2} c_{\alpha_3} t_{c2c1,x}^{c2} - c_{\alpha_2} s_{\alpha_3} t_{c2c1,y}^{c2} + s_{\alpha_2} t_{c2c1,z}^{c2}$ and $b = s_{\alpha_3} t_{c2c1,x}^{c2} + c_{\alpha_3} t_{c2c1,y}^{c2}$.

Eq. (28) can be written for each of the N available combination of poses, giving

$$\boldsymbol{\Phi}\boldsymbol{\zeta} = \boldsymbol{0}, \quad (29)$$

where $\boldsymbol{\Phi} \in \mathbb{R}^{2N \times 5}$. Moreover, $\boldsymbol{\zeta}$ is subject to the constraint imposed by the relation $c_{\alpha_1}^2 + s_{\alpha_1}^2 = 1$, leading to $\zeta_4^2 + \zeta_5^2 = 1$.

It can be noticed that eq. (29) implies that $\boldsymbol{\Phi}$ cannot be a full rank matrix; otherwise, the only solution to (29) would be the trivial one (i.e., $\boldsymbol{\zeta} = \boldsymbol{0}$), which is not possible, given the physical meaning of the parameters in $\boldsymbol{\zeta}$. Hence, $\text{rank}(\boldsymbol{\Phi}) < 5$. On the other hand, it can be shown that, by suitably selecting the poses, $\text{rank}(\boldsymbol{\Phi}) = 4$. In conclusion, $\text{rank}(\boldsymbol{\Phi}) = 4$; thus, $\boldsymbol{\Phi}$ has a 1-dimensional null space, which can be determined by computing the orthonormal (5×5) matrix, $\boldsymbol{V}$, of the input singular vectors. This matrix is a byproduct of the singular values decomposition (SVD) of $\boldsymbol{\Phi}$. In detail, the 5th column of $\boldsymbol{V}$, $\boldsymbol{v}_5$, spans the null space of $\boldsymbol{\Phi}$. Hence, the solution to (29) has the form $\boldsymbol{\zeta}^* = \kappa \boldsymbol{v}_5$, with κ a constant value to be determined. Among the infinite solutions the one of interest is the sole value that satisfies the constraint $\zeta_4^2 + \zeta_5^2 = 1$, which can be easily computed by choosing $\kappa = \frac{1}{\sqrt{v_{5,4}^2 + v_{5,5}^2}}$.

Once r_L is known, it is trivial to obtain r_R and b from (18):

$$\hat{r}_R = -\frac{\hat{\alpha}_R}{\hat{\alpha}_L} \hat{r}_L, \quad \hat{b} = \frac{\hat{r}_R}{\hat{\alpha}_R} \quad \text{or} \quad \hat{b} = -\frac{\hat{r}_L}{\hat{\alpha}_L}. \quad (30)$$

IV. Experiments

Due to space constraint no simulation results will be presented in detail. Nevertheless, several simulations have been carried out, varying, e.g., the number of poses and the sample time T in eq. (25), showing as, for $T = 0.02$s (a realistic value for Khepera III robots), 5-6 poses are enough to get a relative error of 0.1% on the odometry parameters, and 1% on the vehicle-camera roto-translation matrix over a 0.25 average pixel error in the calibration procedure.

The experimental setup is composed by a Khepera III differential drive robot manufactured by K-TEAM Corporation and equipped with a Linux embedded operating system, a standard Logitech QuickCam Web Camera with maximum resolution 640x480, a WIFI communication card that allows to communicate with a standard Pc and two 0.1302deg resolution encoders. The camera calibration is performed via a 6-sided prism, whose base and height dimensions are 0.25m x 0.25m and 0.2m respectively (see Figure 3). On

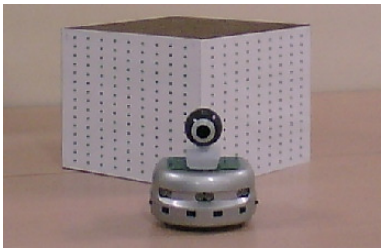

Fig. 3. The experimental setup.

each of the four lateral faces of the calibration box, a CAD designed grid of 135 markers has been attached in such a way the markers positions are known in the box reference frame (i.e. the inertial reference frame).

In order to implement the proposed algorithm, the robot starts from a roughly known initial configuration towards P via points driven only by odometry or by a wireless emulated joystick in the case of completely unknown odometry parameters or long paths; at each via point a picture of the box is taken and the odometry data required by eqs. (23)–(25) are saved; in light of the simulation results, in our experiments a 20 via points path has been chosen (i.e., $P = 20$ poses) letting the robot move many times around the calibration box. With regards to the camera calibration, although the inexpensive chosen model, the average pixel error is 0.5 pixels, corresponding to few millimeters over an average 0.6m x 0.6m scene. Moreover, the mean values of the intrinsic camera parameters are $f_{c,u} = 1013$, $f_{c,v} = 1024$ and $k_r = 2{\cdot}10^{-7}$ with a very small variance around the mean taking into account the camera model.

Figure 4 shows the estimated odometry parameters $\hat{r}_L$, $\hat{r}_R$ and $\hat{b}$ over the number of poses.

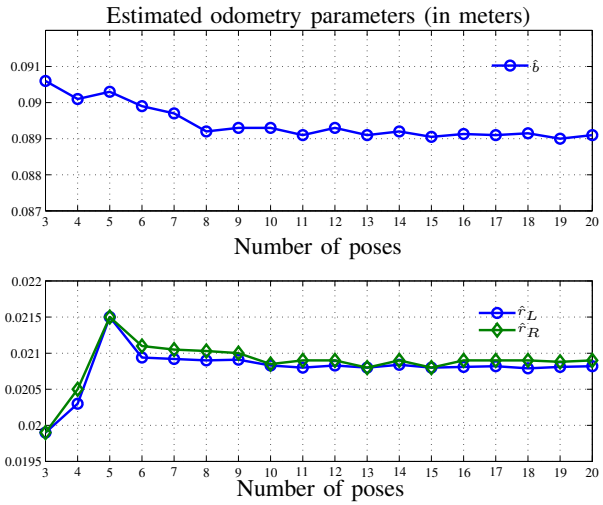

Fig. 4. Odometry parameters estimation over the poses number. On the top: estimated wheels axis length. On the bottom: estimated wheel radii.

It can be noticed how the estimated odometry parameters converge to steady values (i.e. $\hat{r}_L \approx 0.0208$m, $\hat{r}_R \approx 0.0209$m and $\hat{b} \approx 0.0891$m). With regards to the the vehicle-camera roto-translation matrix $\hat{\boldsymbol{A}}_c^v$, Figure 5 shows the translation components $\hat{t}^v_{vc,x}$, $\hat{t}^v_{vc,y}$ and the ZYZ euler angles $\hat{\alpha}_1$, $\hat{\alpha}_2$, $\hat{\alpha}_3$ corresponding to the rotation matrix $\hat{\boldsymbol{R}}_c^v$ over the poses number; the vectors have been shifted towards zero to reduce the y-axis range and achieve a better view of the parameters' trend.

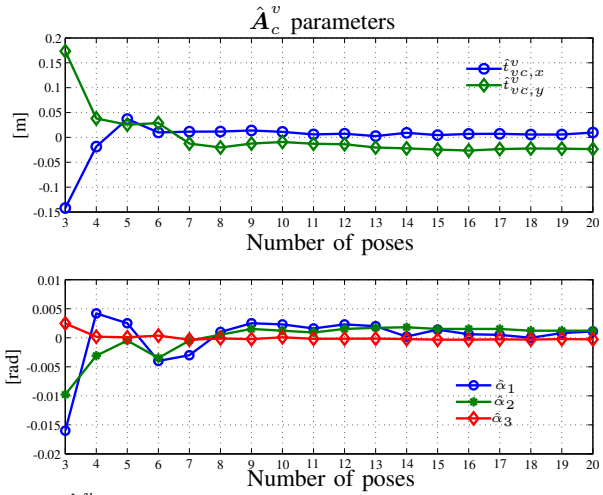

Fig. 5. $\hat{\boldsymbol{A}}_c^v$ parameters over the poses number. On the top: translational component. On the bottom: ZYZ euler angles corresponding to the rotation matrix $\hat{\boldsymbol{R}}_c^v$.

From Figure 5, it can be noticed as, also in this case, the roto-translation matrix $\hat{\boldsymbol{A}}_c^v$ reaches a steady-state value whose good approximation can be

$$\hat{\boldsymbol{A}}_c^v = \begin{bmatrix} -0.0338 & 0.0531 & 0.9980 & 0.0311 \\ 0.0020 & 0.9986 & -0.0531 & -0.0011 \\ -0.9994 & 0.0002 & -0.0339 & 0.1123 \\ 0 & 0 & 0 & 1 \end{bmatrix},$$

where the translational components are expressed in meters and the $\hat{t}^v_{vc,z}$ component has been found constraining the origin of the vehicle reference frame on the inertial x-y plane. Finally, the analysis of the singular values of the matrix $\boldsymbol{\Phi}$ shows as, in our experiments, the ratio σ_5/σ_4 is close to $5 \cdot 10^{-2}$, while $\sigma_4/\sigma_3 \approx 0.7$, confirming that practically $\boldsymbol{\Phi}$ is a rank-4 matrix.

V. Conclusions

In this paper a practical method for the robotic-sensor parameters calibration has been presented. In particular, it allows to simultaneously identify the robot odometry and camera parameters together with the camera pose with respect to the vehicle and without any knowledge of their nominal values. The approach has been proved to be effective also in the case of very inexpensive hardware such as a Khepera III robot and a Logitech web camera.

References

[1] G. Antonelli and S. Chiaverini. Linear estimation of the physical odometric parameters for differential-drive mobile robots. *Autonomous Robots*, 23(1):59–68, July 2007.

[2] G. Antonelli, S. Chiaverini, and G. Fusco. A systematic calibration method for odometry of mobile robots based on the least-squares technique: theory and experimental validation. *IEEE Transactions on Robotics*, 21(5):994–1004, Oct. 2005.

[3] J. Borenstein and L. Feng. Measurement and correction of systematic odometry errors in mobile robots. *IEEE Transactions on Robotics and Automation*, 12(6):869–880, 1996.

[4] Andrea Censi, Luca Marchionni, and Giuseppe Oriolo. Simultaneous maximum-likelihood calibration of robot and sensor parameters. In *Proceedings of the IEEE International Conference on Robotics and Automation (ICRA)*, Pasadena, CA, May 2008.

[5] Y.L. Chang and J.K. Aggarwal. Calibrating a mobile camera's extrinsic parameters with respect toits platform. In *Proceedings of the 1991 IEEE International Symposium on Intelligent Control*, pages 443–448, 1991.

[6] N. Doh, H. Choset, and W.K. Chung. Accurate relative localization using odometry. In *Proceedings 2003 IEEE International Conference on Robotics and Automation*, pages 1606–1612, Taipei, TW, 2003.

[7] N.L. Doh, H. Choset, and W.K. Chung. Relative localization using path odometry information. *Autonomous Robots*, June 2006.

[8] S. Hutchinson, G.D. Hager, and P.I. Corke. A tutorial on visual servo control. *IEEE Transactions on Robotics and Automation*, 12(5):551–570, 1996.

[9] A. Kelly. General solution for linearized systematic error propagation in vehicle odometry. In *Proceedings 2001 IEEE/RSJ International Conference on Intelligent Robots and Systems*, pages 1938–1945, Maui, HI, Nov. 2001.

[10] A. Kelly. General solution for linearized stochastic error propagation in vehicle odometry. In *Preprints 15th IFAC World Congress*, Barcelona, Spain, July 2002.

[11] R.Y. Tsai R.K. Lenz. A new technique for fully autonomous and efficient 3D robotics hand/eye calibration. *IEEE Transactions on Robotics and Automation*, 5(3):345–358, 1989.

[12] K. Madsen, H.B. Nielsen, and O. Tingleff. *Methods for Non-Linear Least Squares Problems*. Technical University of Denmark, Lyngby, DK, 2004.

[13] A. Martinelli. The accuracy on the parameter estimation of an odometry system of a mobile robot. In *Proceedings 2002 IEEE International Conference on Robotics and Automation*, pages 1378–1383, Washington, DC, May 2002.

[14] A. Martinelli. The odometry error of a mobile robot with a synchronous drive system. *IEEE Transactions on Robotics and Automation*, 18(3):399–405, 2002.

[15] F.C. Park and B.J. Martin. Robot sensor calibration: solving AX=XB on the Euclidean group. *IEEE Transactions on Robotics and Automation*, 10(5):717–721, 1994.

[16] L. Sciavicco and B. Siciliano. *Modeling and Control of Robot Manipulators*. Springer-Verlag, London, UK, 2nd edition, 2000.

[17] C.M. Wang. Location estimation and uncertainty analysis for mobile robots. In *Proceedings 1988 IEEE International Conference on Robotics and Automation*, pages 1230–1235, Philadelphia, PA, 1988.